Submitted to Physical Review Letters

Differential Photoelectron Holography: A New Approach for Three-Dimensional Atomic Imaging

S. Omori,[1,2] Y. Nihei,[1] E. Rotenberg,[3] J. D. Denlinger,[3] S. Marchesini[2], S. D. Kevan,[4] B. P. Tonner,[5]
M. A. Van Hove[2,3,6] and C. S. Fadley[2,6]
[1]*Institute of Industrial Science, University of Tokyo,*
Tokyo 153-8505, Japan
[2]*Materials Sciences Division, Lawrence Berkeley National Laboratory,*
Berkeley, California 94720
[3]*Advanced Light Source, Lawrence Berkeley National Laboratory,*
Berkeley, California 94720
[4]*Department of Physics, University of Oregon,*
Eugene, Oregon 97403
[5]*Department of Physics, University of Central Florida,*
Orlando, Florida 32816
[6]*Department of Physics, University of California,*
Davis, California 95616

We propose differential holography as a method to overcome the long-standing forward-scattering problem in photoelectron holography and related techniques for the three-dimensional imaging of atoms. Atomic images reconstructed from experimental and theoretical Cu 3p holograms from Cu(001) demonstrate that this method suppresses strong forward-scattering effects so as to yield more accurate three-dimensional images of side- and back-scattering atoms. Our results further suggest that even forward-scattering atoms can at least be approximately imaged if appropriate **k** sampling is chosen.

61.14.-x, 42.40.-i

Holography [1] is a well-known method of recording both the amplitudes and phases of waves scattered by an object illuminated with coherent radiation, and using this information to directly construct a three-dimensional image of the object. Szöke [2] first suggested that highly coherent outgoing waves from atomically localized sources of photoelectrons, fluorescent x-rays, and γ rays could be used to achieve atomic-scale holography. This idea was initially demonstrated theoretically for the case of photoelectrons by Barton [3], and then extended into a multi-energy format by Barton and Terminello and by Tong and co-workers [4]. By now several experimental approaches to such atomic-resolution holography have been demonstrated, including photoelectrons [5-8], Auger electrons [9], Kikuchi electrons [10], diffuse low-energy electrons (LEED) [11], fluorescent x-rays in either a direct mode [12] or a time-reversed multi-energy mode [13], γ rays [14], and bremsstrahlung x-rays [15].

Among these methods, photoelectron holography (PH) has the advantages of being capable of studying the local

atomic structure around each type of emitter without requiring long-range order and of distinguishing emitters through core-level binding-energy shifts [8]. Photoelectron holograms also show strong modulations of up to ±50%, so such effects are easily measurable. However, atomic images of PH can suffer from serious aberrations due to the strong non-optical nature of electron scattering. The atomic scattering factor f is also a highly anisotropic function of scattering angle, and can depend strongly on electron kinetic energy E_k. In particular, as E_k increases above a few hundred eV, f becomes more and more significant in the forward direction, resulting in a strong forward-scattering (FS) peak [16] that can induce image aberrations. At higher energies, images of FS atoms tend to be elongated sausage-like features [6]. Beyond this, PH also can suffer from multiple-scattering effects due to the strength of the scattering.

Various reconstruction algorithms and measurement methods [4,5,7,17] have been proposed to correct for the anisotropic f and multiple scattering, some of which can be summarized as

$$U(\mathbf{r}) = \left| \int Wc(\mathbf{k}) \exp[-ikr + i\mathbf{k}\cdot\mathbf{r}] d^3\mathbf{k} \right|^2, \qquad (1)$$

where U is the image intensity at position $\mathbf{r}$, c is the normalized hologram based on intensities measured over three-dimensional $\mathbf{k}$ space, and the function or operator W permits describing the difference between algorithms, with W=1 in the original multi-energy formulations [4]. One alternative algorithm [5] sets $W = f^{-1}\left(k, q_{\mathbf{r}}^{\mathbf{k}}\right)$ so as to divide out the anisotropic f, where $q_{\mathbf{r}}^{\mathbf{k}}$ is the scattering angle between $\mathbf{r}$ and $\mathbf{k}$. Another algorithm [7] is based on the more nearly optical-like back scattering (BS) of electrons, with the scattering phase being nearly constant and $|f|$ only weakly varying as a function of $q_{\mathbf{r}}^{\mathbf{k}}$, by contrast with the forward direction. Thus, a window function for W that limits the integral in Eq. (1) to be in a small cone of $\hat{\mathbf{k}}$ around $-\mathbf{r}$ is chosen to emphasize the imaging of BS atoms. Although successful in several applications [7,18], it is difficult if not impossible to apply this small-cone method to many systems where the imaging of FS or even side-scattering (SS) atoms is of crucial importance, such as epitaxial films and buried interfaces. In fact, imaging of "bulk" atoms surrounded by forward- and back-scattering atoms via PH has proven to be especially difficult [cf. Figs. 7-9 in ref. 8], with most successful applications being to emitters in the first couple of layers near a surface.

To overcome the difficulties associated with strong and anisotropic FS, we propose in this Letter "differential holography". By simply replacing c in Eq. (1) by its k-derivative (i.e. $W = \partial/\partial k$) or more conveniently by a numerical difference between two c's at different energies ($dc = c(k + dk) - c(k)$), FS effects can be greatly suppressed. We have applied this method to both experimental and theoretical multi-energy holograms for Cu 3p emission from Cu(001), and show that this provides images that are improved over prior work in several respects. Applications of this approach in other electron-based holographies also seem possible.

To avoid confusion with other methods in PH, we also note that “derivative” PH has been proposed and used successfully by Chiang and co-workers [18], and this also is based on measurements of photoelectron intensity $I(\mathbf{k})$ at two different energies. However, the purpose here is to eliminate uncertainties in I due to the variation of experimental conditions by first taking logarithmic derivatives $[\partial I/\partial k]/I$ that are then reintegrated into “self-

normalized" intensities; thus, it is still finally c that is used in Eq. (1).

The principle of differential photoelectron holography (DPH) is as follows. We consider the single-scattering expression of c for an emitter-scatterer pair spaced by a vector $\mathbf{r}$ [16]:

$$c(\mathbf{k}) = \frac{I - I_0}{I_0} \approx \frac{2|f(k, q_{\mathbf{r}}^{\mathbf{k}})|}{r} \cos\left[kr\left(1 - \cos q_{\mathbf{r}}^{\mathbf{k}}\right) + j\left(k, q_{\mathbf{r}}^{\mathbf{k}}\right)\right], \tag{2}$$

where I_0 is the intensity that would be observed without atomic scattering, c is defined in the usual way and j is the scattering phase. If δk is sufficiently small so that $\delta|f|/|f| \ll 1$, where $\delta|f|$ is the change in $|f|$, the difference of two holograms at $k_{\pm} = k \pm \delta k/2$ can be written in a similar form to Eq. (2) as:

$$\delta c(\mathbf{k}) = c\left(k_+ \hat{\mathbf{k}}\right) - c\left(k_- \hat{\mathbf{k}}\right) \approx -\frac{2|f_{\text{eff}}|}{r} \sin\left[kr\left(1 - \cos q_{\mathbf{r}}^{\mathbf{k}}\right) + \bar{j}\left(k, q_{\mathbf{r}}^{\mathbf{k}}\right)\right], \tag{3}$$

where the direction $\hat{\mathbf{k}}$ is defined by angles q and f, the "effective" scattering amplitude is defined as $|f_{\text{eff}}| = 2|f|\sin\left[\delta kr\left(1 - \cos q_{\mathbf{r}}^{\mathbf{k}}\right)/2 + \delta j/2\right]$, and $\bar{j}$ is the average of j's at $k_{\pm}$. In the FS region where $q_{\mathbf{r}}^{\mathbf{k}} \to 0$, $|f_{\text{eff}}|$ is thus very small, approaching zero in the limit of $\delta j \to 0$. If δk is also small, $|f_{\text{eff}}|$ is proportional to r; thus, DPH not only suppresses the FS effects, but also enhances the imaging of distant atoms. However, $\bar{j}$ still remains in the holographic oscillation of Eq. (3), and this could be the origin of small image position shifts. In Fig. 1, $|f|$ and $|f_{\text{eff}}|$ are plotted as a function of $q_{\mathbf{r}}^{\mathbf{k}}$ for Cu-Cu nearest neighbors (r=2.56 Å). For k=4.6 Å^{-1} and δk=0.2 Å^{-1}, $|f_{\text{eff}}|$ is significant only in the region of $q_{\mathbf{r}}^{\mathbf{k}}$ >~90°. Therefore, the imaging of SS and BS atoms is expected, while it will be difficult for this case to image FS atoms. On the other hand, for k=8.8 Å^{-1} and a larger fractional δk=1.0 Å^{-1}, $|f_{\text{eff}}|$ is significant not only in the BS region but also in the range of $q_{\mathbf{r}}^{\mathbf{k}}$ ~30°-90°. Since it is well known that near-neighbor FS diffraction fringes extend out beyond 30° [16,19], we might expect the latter choice to also permit imaging FS atoms. In this way, the relative sensitivity of DPH to SS and FS atoms can be "tuned" by selecting the range and step width of k scans. Finally, we note that the suppression of multiple-scattering effects by means of a transform over a volume in $\mathbf{k}$ space via Eq. (1) is well known in normal multi-energy PH [4] and this suppression will be equally present in DPH. If anything, the inherent elimination of strong FS effects in DPH should lead to even better multiple-scattering suppression.

To demonstrate DPH experimentally, photoelectron holograms from Cu(001) were measured at undulator beamline 7.0 of the Advanced Light Source at the Lawrence Berkeley National Laboratory. Photoelectron spectra for Cu 3p emission were collected at 25 energies over k=4.5-9.3 Å^{-1} (E_k=77-330 eV) with a constant step of δk=0.2 Å^{-1} (δE_k =7-14 eV), along 65 different directions over a symmetry-reduced 1/8 of the total solid angle above the specimen, and with a polar angle range from q=0° (surface normal) to 70°. A total of 1625 unique intensities were thus measured. The photoelectron intensity $I(k,q,f)$ was fitted by low-order polynomials to obtain the smooth

background intensity [8,20]:

$$I_0(k,q) = (a_0 + a_1 k + a_2 k^2)(b_0 + b_1 \cos q + b_2 \cos 3q). \quad (4)$$

Three kinds of c were obtained from this fitting: c_A by fitting the second factor of Eq. (4) to a scanned-angle pattern $I_k(q, f)$ at each fixed k [6], c_B by fitting the first factor to a scanned-energy curve $I_{\hat{\mathbf{k}}}(k)$ at each fixed direction $\hat{\mathbf{k}}$ [7] and c_C by fitting both factors to the full data set of $I(k,q, f)$ at one time, with the last expected to be the most accurate from an *a priori* point of view [8]. The k-differences from c_C were also used for DPH in what we will term Method D (i.e., $c_D = dc_C$). The exact method of I_0 subtraction has been the origin of some controversy concerning the fidelity of reconstructed images. It has been suggested [10] that Method B has an advantage over Method A in that low-frequency oscillations due to FS events in $I_{\hat{\mathbf{k}}}(k)$ are automatically removed. However, this also means that the I_0 from Method B inherently deviates from the true I_0 defined as the intensity without scattering, especially in the FS direction. In addition, since each $I_{\hat{\mathbf{k}}}(k)$ is independently normalized without considering the continuity of c in the whole sampled **k** space, Method B could degrade holographic fringes in $I_k(q, f)$. Similarly, Method A could degrade holographic oscillations in $I_{\hat{\mathbf{k}}}(k)$. By contrast, Method C takes into account the continuity of c over the whole data set, but the FS peaks remain in c_C. Thus, the comparison of Methods A-D is of great interest and a critical test for DPH. The simple original transform of Eq. (1) was used for all four data sets; but to avoid spurious features due to the abrupt truncation of the integral in Eq. (1), W was taken to be the product of a Gaussian function of k and a Hanning function $\cos^2 q$, with an additional multiplication by r to make atoms at larger distances more visible.

Figure 2 shows atomic images reconstructed from c_A-c_D in the vertical (100) plane of Cu(001). BS atoms of type 1 are imaged in all four methods, but the degree to which other atoms of types 2-7 are imaged varies greatly. In Methods A and C, only elongated features related to FS effects from atoms 6 and 7 are observed above z_c=–0.5 Å (the arbitrary location of a change in image multiplication). This is consistent with a previous PH study of W(110) [8], in which Method C was used. By contrast, it has been reported in one of the earliest PH studies using Method A [6] that FS atoms of type 5 have been imaged from Cu 3p holograms for Cu(001) obtained at 9 energies. Even if possible differences in the two sets of experimental data are taken into account, it is difficult to conclude from our results that the images of these FS atoms can be resolved from the strong FS artifacts via Method A. Below z_c and with higher image amplification, several peaks near the BS atomic positions 1-3 are observable for Methods A and C among various strong artifacts, but only with the help of large scale factors of 46 and 29, respectively.

In Methods B and D, image intensities are stronger in the BS region, with the relative image amplification factors being reversed in sense and smaller at x5 compared to A and C. In Method D, a strong, somewhat elongated peak is observed at the FS atomic position 6, with weaker features that appear to be associated with atoms 7 also present in the corners of the image. In both B and D, two strong peaks are observed at the SS positions 4 above z_c and five peaks are observed at the BS positions below z_c for atoms 1-3. However, the most intense features in Method B are the artifacts between the two nearest BS atoms of type 3. In fact, neglecting the difference in the scale factors, the image below z_c from Method B is only comparable in quality with that from Method C. In Method D, by contrast, the

five strongest peaks below z_c are of roughly equal intensity and correspond reasonably well to the near-neighbor BS atoms. Therefore, we find Method D to be the most robust for imaging both SS and BS atoms (as well as to some degree also FS atoms of type 6), even if there are shifts in position of approximately 0.1 Å for type 1, 0.6 Å for 2, and 0.3 Å for 3. Such peak shifts relative to the true atomic positions, as observed in all methods, can be attributed to the neglect of corrections for both the scattering phase and the inner potential, which have not been included here. For comparison with experiment, we have also performed multiple-scattering simulations of $I(\mathbf{k})$, using a cluster method fully described elsewhere [21]. The theoretical I_0 was obtained simply as the square of the zeroth-order wave function without scattering. Images reconstructed from the theoretical c and dc via Methods C and D are shown in Figs. 2(e) and (f), and they can be compared with Figs. 2(c) and (d), respectively. The main features in Figs. 2(c) and (d) are well reproduced by our simulations, although the artifacts between the images of atoms 3 are much stronger in experiment for Method C, and the relative intensity in the region of FS atom 6 is stronger in experiment for Method D. Even though the ideal c was used for image reconstruction, Fig. 2(e) shows that no atomically-resolved SS or FS peaks are observable with Method C above z_c. Therefore, the corresponding artifacts in Fig. 2(c) are not purely due to the uncertainties in the experimental data and any errors in the I_0 subtraction, but largely have their origin in the algorithm. On the other hand, Fig. 2(f) based on Method D exhibits well-resolved peaks at the SS and BS atomic positions. Since there are no artifacts below z_c in Fig. 2(f), the artifacts below z_c in Fig. 2(d) are by contrast considered to be purely due to the experimental noise and other non-idealities in the data analysis (e.g. I_0 determination).

We have also generated full three-dimensional atomic images from the experimental data via c_D, although length limitations prevent showing these here. In these images, we find in addition to the atoms of types 1-4 and 6 in Fig. 2, two other types of near-neighbor BS and SS atoms located in the vertical (110) plane (denoted types 2' and 4' and situated in the same horizontal layers as 2 and 4, respectively). All of these atoms are reasonably well reconstructed, with only a few, such as 2, being significantly shifted in position, but most within a few tenths of an Å of the correct positions in all directions. Even though four weaker artifacts are observed at radii inside of the positions of atoms 3, the three-dimensional image quality is much better than any of the previous PH images of bulk substrate emission [6,8]. The FS atom 6 is elongated as expected, but nonetheless has its brightest point rather close to the true location. The overall positional errors for all of the atoms compared to the known Cu lattice can be summarized as (radial location shift in xy)/(vertical location shift in z), and are: 0.0 Å/0.1 Å for atoms 1, 0.6 Å/0.1 Å for atoms 2, 0.3 Å/0.1 Å for atoms 2', 0.2 Å/0.1 Å for atoms 3, 0.1 Å/0.0 Å for atoms 4, 0.3 Å/0.0 Å for atoms 4', and 0.0 Å/0.4 Å for the FS atom 6. As a further indication of the overall image quality obtained by DPH, the reader is referred to an animated comparison of 3D images for the four approaches of Fig. 2(a)-(d), in which DPH is alone in imaging approximately 15 near-neighbor atoms [22].

Finally, we compare DPH with a very recently introduced approach for PH termed near-node holography [23], in which FS effects are suppressed by using a special experimental geometry with electron exit nearly perpendicular to light polarization. Although this technique is promising, DPH has the advantages that it does not require a special experimental geometry or s-subshell-like form for the photoelectric cross section, that it seems to yield images of as good or better quality [22,23], and that it can be used in other types of holography in which polarization cannot be varied.

In summary, we have demonstrated differential photoelectron holography (DPH) as a powerful method for overcoming the FS problem in PH and enhancing image quality for any kind of system in which FS can arise, as for example, bulk emission, buried interfaces and complex overlayers. This method should also be helpful in other types of electron holography in which energy can be stepped in a controlled way (e.g. Kikuchi [10] or LEED [11] holography). The reconstructed images from experimental and theoretical data for Cu 3p/Cu(001) demonstrate that DPH is successful in suppressing the FS effects so as to image SS, BS (and to some degree also FS) atoms with accuracies of -0.1-0.6 Å. In addition, theoretical considerations as shown in Fig. 1 suggest that the imaging of FS atoms can be improved if appropriate experimental conditions of **k** sampling are chosen.

This work was supported in part by the Director, Office of Energy Research, Basic Energy Science, Materials Sciences Division of the U. S. Department of Energy under Contract No. DE-AC03-76SF00098. S.O. and Y.N. also acknowledge the support of the Japan Society for the Promotion of Science (Grant No. JSPS-RFTF 98R14101).

[1] D. Gabor, Nature **161**, 777 (1948).

[2] A. Szöke, in *Short Wavelength Coherent Radiation: Generation and Applications*, AIP Conf. Proc. No. 147, edited by D. T. Attwood and J. Boker (AIP, New York, 1986), p. 361.

[3] J. J. Barton, Phys. Rev. Lett. **61**, 1356 (1988).

[4] J. J. Barton, Phys. Rev. Lett. **67**, 3106 (1991); J. J. Barton and L. J. Terminello, in *Structure of Surfaces III*, edited by S. Y. Tong, M. A. Van Hove, X. Xide and K. Takayanagi (Springer-Verlag, Berlin, 1991), p. 107; S. Y. Tong, H. Li and H. Huang, Phys. Rev. Lett. **67**, 3102 (1991).

[5] B. P. Tonner *et al*., Phys. Rev. B **43**, 14423 (1991).

[6] L. J. Terminello, J. J. Barton and D. A. Lapiano-Smith, Phys. Rev. Lett. **70**, 599 (1993).

[7] S. Y. Tong, H. Li and H. Huang, Phys. Rev. B **51**, 1850 (1995); H. Wu and G. J. Lapeyre, *ibid*. **51**, 14549 (1995).

[8] P. M. Len *et al*., Phys. Rev. B **59**, 5857 (1999).

[9] D. K. Saldin, G. R. Harp and X. Chen, Phys. Rev. B **48**, 8234 (1993).

[10] C. M. Wei, I. H. Hong and Y. C. Chou, Surf. Rev. Lett. **1**, 335 (1994).

[11] D. K. Saldin and P. L. DeAndres, Phys. Rev. Lett. **64**, 1270 (1990); K. Reuter *et al*., Phys. Rev. B **58**, 4102 (1998).

[12] M. Tegze and G. Faigel, Europhys. Lett. **16**, 41 (1991); P. M. Len *et al*., Phys. Rev. B **50**, 11275 (1994).

[13] T. Gog *et al*., Phys. Rev. Lett. **76**, 3132 (1996).

[14] P. Korecki, J. Korecki and T. Slezak, Phys. Rev. Lett. **79**, 3518 (1997).

[15] S. G. Bompadre, T. W. Petersen and L. B. Sorensen, Phys. Rev. Lett. **83**, 2741 (1999).

[16] C. S. Fadley, Surf. Sci. Rep. **19**, 231 (1993).

[17] T. Greber and J. Osterwalder, Chem. Phys. Lett. **256**, 653 (1996).

[18] D. –A. Luh, T. Miller and T. –C. Chiang, Phys. Rev. Lett. **81**, 4160 (1998).

[19] S. Omori, T. Kozakai and Y. Nihei, Surf. Rev. Lett. **6**, 1085 (1999).

[20] P. M. Len, Ph.D. thesis, University of California, Davis (1997).

[21] Y. Chen *et al*., Phys. Rev. B **58**, 13121 (1998); MSCD photoelectron diffraction program package from http://electron.lbl.gov/mscdpack/mscdpack.html.

[22] Animated rotating images in 3D showing the four experimental cases of Figs. 2(a)-2(d) also appear at http://electron.lbl.gov/marchesini/dph/.

[23] J. Wider *et al*., Phys. Rev. Lett. **86**, 2337 (2001).

Figure Captions

Fig. 1- Comparison of the usual scattering amplitude $|f|$ and the effective scattering amplitude of differential holography $|f_{\text{eff}}|$, calculated for Cu-Cu nearest neighbors (r=2.56 Å) as a function of scattering angle $q_{\mathbf{r}}^{\mathbf{k}}$ for two different sets of k and δk in taking the differential of c: (a) k = 4.6 Å^{-1} (81 eV), δk = 0.2 Å^{-1} (7 eV) and (b) k = 8.8 Å^{-1} (295 eV), δk = 1.0 Å^{-1} (67 eV). The final strong forward-scattering data points of $|f|$ at the right of panel (b) are truncated. We have confirmed numerically that Eq. (3) is a good approximation even in the case of (b), where δk has a larger fractional value.

Fig. 2(color)- Atomic images in the vertical (100) plane of Cu (001) reconstructed from Cu 3p holograms obtained by Methods A–D, as described in the text. The emitter and scatterer positions are indicated by squares and circles, respectively, and various near-neighbor atoms are numbered. Image intensities above or below z_c=–0.5 Å have been rescaled by the factor shown in each panel, with this factor being determined so as to make the maximum intensities above and below z_c equal. *Experimental images* (a) Image obtained by Method A: normal holography via Eq. (1) with I_0 determined by fitting the angular variation of Eq. (4) at each k value. (b) Image obtained by Method B: normal holography with I_0 determined by fitting the k variation of Eq. (4) along each direction. (c) Image obtained by Method C: normal holography with I_0 determined by fitting both the angular and k variation in Eq. (4). (d) Image obtained by Method D: differential holography with I_0 determined by fitting both the angular and k variation in Eq. (4) and then using δc in Eq. (1). *Theoretical images* (e) As (c) but theoretical. (f) As (d) but theoretical.

Additional reference data:

Figure A- Three-dimensional Cu(001) atomic image reconstructed from the experimental holograms by Mathod D--differential holography with a 3D I_0 function. Image intensities above z_c = 0.5 Å have been multiplied by a factor of 4, and isosurfaces at 50 % of the maximum intensity are shown together with five slices at z=0 (the emitter plane), ±1.81 (the first nearest layers) and ±3.62 Å (the second nearest layers). Reconstructed forward-, side- and back-scattering atoms are numbered, and the corresponding atoms in the crystal model are indicated in the inset. Only the four features labeled A inside the atomic peaks 3 are weak artifacts that cannot be connected with a specific atom. (Can be compared directly to Fig. 3 in Wider et al., Phys. Rev. Lett. 86, 2337 (2001).)

Figure B- Atomic images in the vertical (100) plane of Cu (001) reconstructed from theoretical Cu 3p holograms: (a) Image obtained via normal holography. As Fig. 2(e) in the manuscript, but based on the different **k**-space sampling used in the previous PH study by Terminello *et al*. (PRL **70**, 599 (1993)). (d) Image obtained via differential holography. As Fig. 2(f) in the manuscript, but based on the different **k**-space sampling used in the previous PH study by Terminello *et al*. Note the improved imaging of forward scattering atoms via DPH.

(a) k=4.6Å^{-1} (81eV), dk = 0.2Å^{-1} (dE = 7 eV)

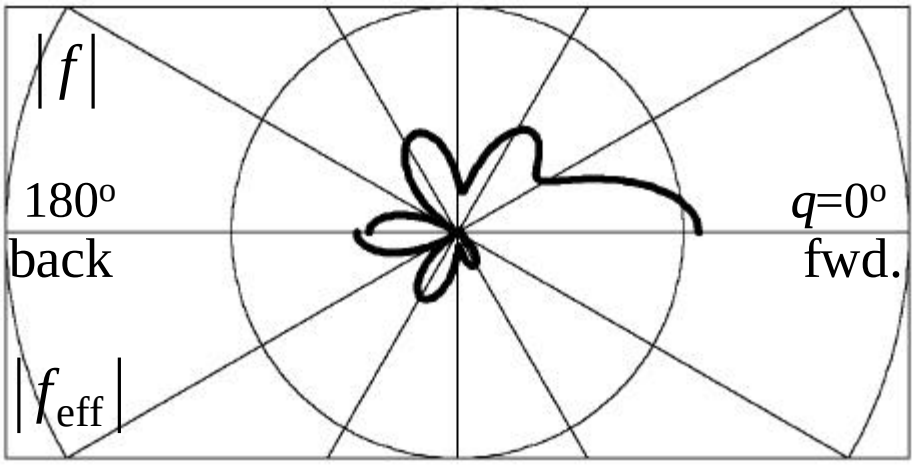

(b) k=8.8Å^{-1} (295eV), dk = 1.0Å^{-1} (dE = 67eV)

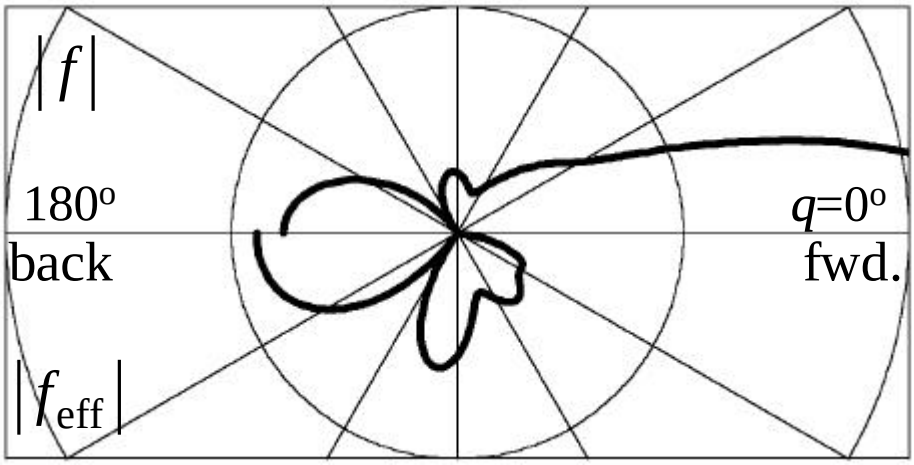

Fig. 1 (S. Omori et al.)

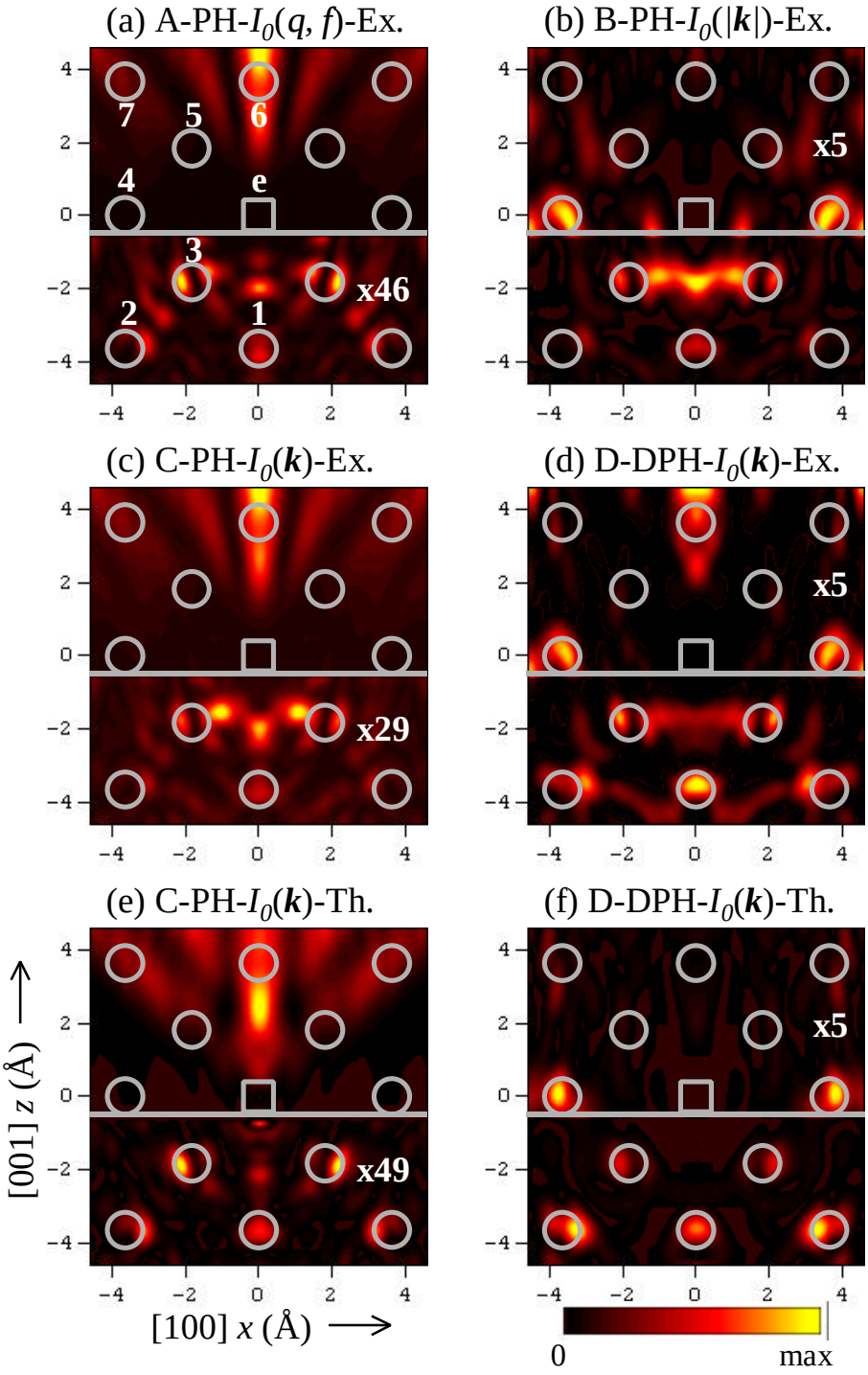

Fig. 2 (S. Omori et al.)

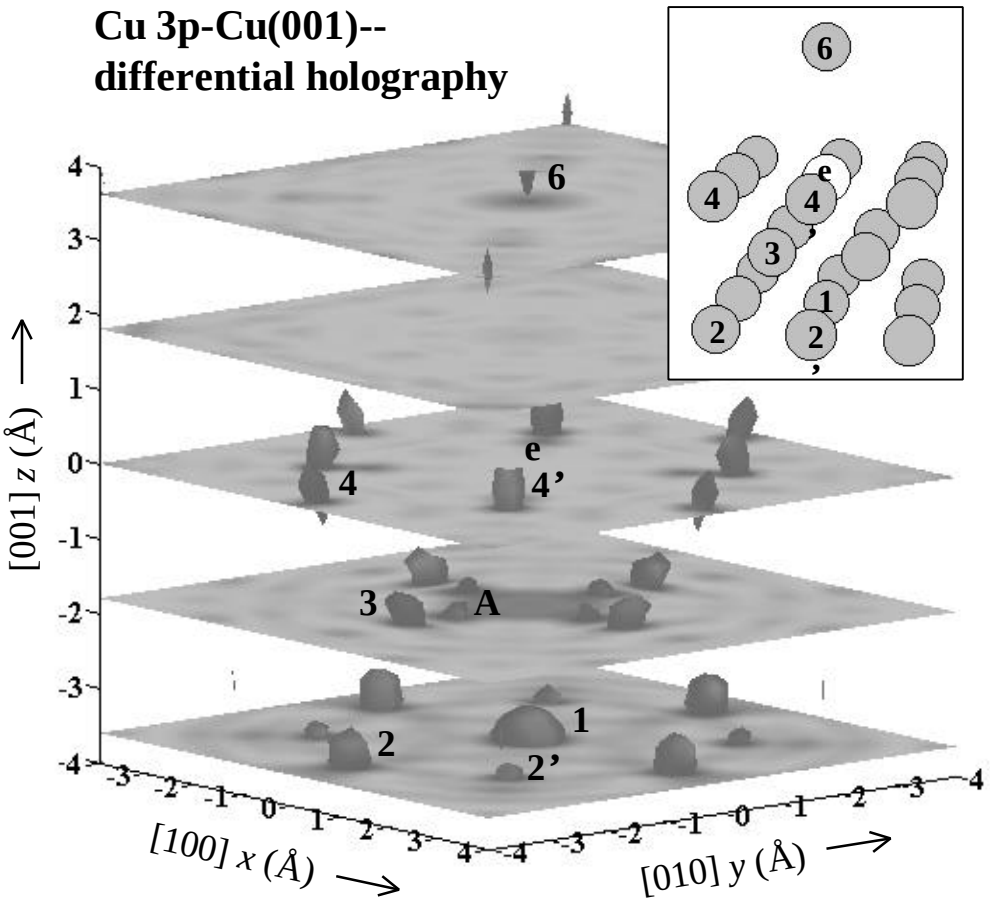

Fig. A(for reference) (S. Omori et al.)

(a) C-PH-$I_0(\boldsymbol{k})$-Theo.

(b) D-DPH-$I_0(\boldsymbol{k})$-Theo.

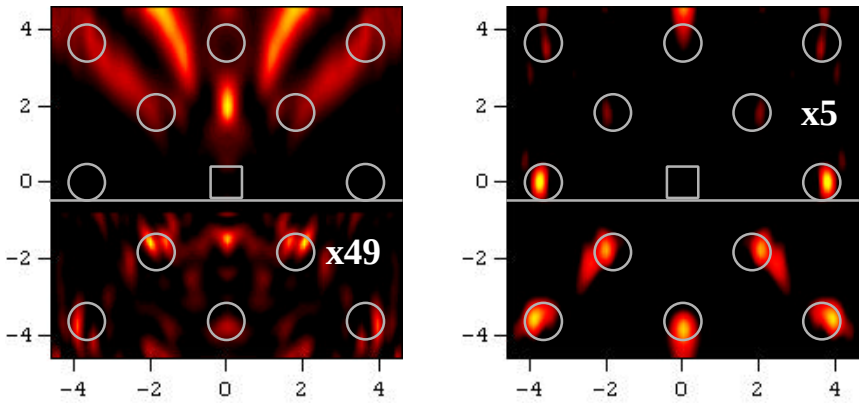

Fig. B(for reference) (S. Omori et al.)